PNAS RESEARCH ARTICLE | NEUROSCIENCE

Frontotemporal network contribution to occluded face processing

Jalaledin Noroozi[a,b], Ehsan Rezayat[c], and Mohammad-Reza A. Dehaqani[d,1]

Affiliations are included on p. 11.

Edited by David A. Leopold, National Institute of Mental Health, Bethesda, MD; received April 13, 2024; accepted October 14, 2024 by Editorial Board Member J. Anthony Movshon

Primates are known for their exceptional ability to recognize faces. However, we still have much to learn about how their brains process faces when they are partially hidden. When we cover parts of a face, it affects how our brains respond, even though we still perceive the face as a whole. This suggests that complex brain networks are at work in understanding partially hidden faces. To explore this further, we studied two brain regions, the ventrolateral prefrontal cortex (vlPFC) and the inferior temporal cortex (ITC), while showing primate images of faces with parts occluded. We found that vlPFC neurons were more active when faces were partially covered, while ITC neurons preferred fully visible faces. Interestingly, the ITC seemed to process occluded faces in a separate phase after the vlPFC responded. Our research revealed a coordinated effort between these brain regions based on the level of facial obstruction. Specifically, the vlPFC seemed to play a crucial role, driving the representation of occluded faces in the later phase of ITC processing. Importantly, we also found that the brain processes occluded faces differently from those that are fully visible, suggesting specialized mechanisms for handling these situations. These findings highlight the importance of feedback from the vlPFC in understanding occluded faces in the ITC region of the brain. Understanding these neural processes not only enhances our understanding of how primates perceive faces but also provides insights into broader aspects of visual cognition.

face recognition | occlusion | inferior temporal cortex | ventrolateral prefrontal cortex

Significance

Recognizing faces can be challenging when they are partially occluded, but the neural mechanisms underlying this process remain unclear. We investigated two vital brain regions, the ventrolateral prefrontal cortex (vlPFC) and the inferior temporal cortex (ITC), to elucidate this phenomenon. Our findings revealed that in the presence of partially occluded faces, the vlPFC exhibits heightened activity, whereas the ITC demonstrates a preference for intact facial stimuli. Intriguingly, the ITC appears to decode occluded facial features subsequent to vlPFC processing, indicative of collaborative neural processing. This underscores the pivotal role of vlPFC facilitation in the ITC's comprehension of occluded facial cues and reveals unique insights into neural processing mechanisms. Deciphering these processes enhances our understanding of visual perception and cognitive processing.

Face recognition is a remarkable cognitive ability in primates, allowing them to accurately detect and respond to faces despite variations in facial appearance (1–3). Face occlusion poses a critical challenge to social interactions, obstructing successful recognition (4, 5). Despite extensive research on the neural mechanisms of face representation, the neural processes underlying the recognition of partially occluded faces remain poorly understood. Understanding these processes is crucial for comprehending the mechanisms involved in robust face recognition.

The inferior temporal cortex (ITC) contains important neurons involved in face detection and processing (6–9). Previous research indicates that partial occlusion affects IT neuron responses in various ways (10, 11). Specifically, 60% of IT neurons show increased activity to partially occluded geometrical shapes, with responses influenced more by the occlusion area than by the occluder's color or shape. In contrast, a smaller group of highly shape-selective neurons responds best to complete shapes (10). Additionally, while IT neurons maintain shape selectivity with both static and moving occluders, their responsiveness decreases with greater occlusion and requires longer stimulus durations compared to nonoccluded shapes (11). Similarly, research on V4 neurons reveals that their shape selectivity also diminishes with increased occlusion, although some neurons retain their selectivity even with significant occlusion levels (12). In the PL brain area, many cells respond strongly to faces, particularly when an eye is visible. However, the response of these cells decreases if the eye is occluded, paralleling the decrease seen when the entire face is occluded. This suggests a direct and consistent processing of face features across different brain areas (13).

Similarly, the ventrolateral prefrontal cortex (vlPFC) in macaque monkeys also has specific regions dedicated to facial processing (14). In addition to the role of the vlPFC in high-level cognitive function, it has been demonstrated that the vlPFC plays a particularly crucial role when stimuli are ambiguous (15). It has been proposed that the activity of the vlPFC plays a role in representing occluded images in the ITC (16, 17). Electrophysiological studies demonstrate that the coordination between ITC and vlPFC activity is crucial for comprehending challenging visual stimuli (18–21). While existing research underscores

Author contributions: J.N. and M.-R.A.D. designed research; J.N. and E.R. performed research; J.N. and M.-R.A.D. contributed new reagents/analytic tools; J.N. and M.-R.A.D. analyzed data; and J.N. and M.-R.A.D. wrote the paper.

The authors declare no competing interest.

This article is a PNAS Direct Submission D.A.L. is a guest editor invited by the Editorial Board.

[1]To whom correspondence may be addressed. Email: dehaqani@ut.ac.ir.

This article contains supporting information online at https://www.pnas.org/lookup/suppl/doi:10.1073/pnas.2407457121/-/DCSupplemental.

Published November 18, 2024.

the significance of these areas, the collaboration between the two in processing occluded visual information and the dissociation of occluded face processing from face identity processing remain unclear.

Although theoretical and brain signal studies have predominantly focused on feedforward architecture (22, 23), there is extensive evidence supporting the role of feedback signaling in visual processing (16, 17, 23). However, little is known about the collaboration of vlPFC feedback in occluded face processing at the ITC. In this study, we aimed to investigate the frontotemporal networks that contribute to the representation of challenging occluded faces. We employed a large dataset of occluded face images and simultaneously recorded neural activity from two regions of interest, namely the vlPFC and the ITC.

Our study reveals distinctive neural response patterns in the vlPFC and ITC during occluded face processing. We observed delayed processing in ITC neurons following vlPFC responses, particularly for highly occluded faces. Furthermore, we demonstrated retrograde communication between the ITC and vlPFC, highlighting feedback's crucial role in resolving occluded face processing. We found higher frontotemporal coordination for processing of faces with higher degree of occlusion, emphasizing the importance of long recurrent connections for effective occluded face processing. Overall, our findings argue that vlPFC feedback is critical for partially occluded face representation and contributes to the development of more robust computational models for occluded face processing.

Results

In this study, we recorded neural activity from two single electrodes simultaneously, targeting the ITC and vlPFC (110 sessions, 184 neurons in the ITC, 161 neurons in the vlPFC, 2 monkeys). Initially, we used the selectivity task to identify the face-selective neurons, and then we conducted the main task of our study on these neurons. We measured the neuronal response while the monkeys were performing a passive task (Fig. 1*A*), wherein the monkey was required to maintain its gaze fixed on a specific point. In our study, the main task involved presenting the stimulus for 350 ms with 500 ms intervals. The monkeys received a reward every 3 s for maintaining their gaze on the fixation point. In our study, we used one-way ANOVA to evaluate the representation of complex features in the ITC and vlPFC regions (Fig. 1*B*). We found that neurons in the ITC exhibited a more pronounced representation of these features compared to neurons in the vlPFC, highlighting the ITC's specialized role in visual object recognition.

First, we tested how different artificial occluders affected neuronal responses. *SI Appendix*, Fig. S12 shows that none of the three types of occluders caused a significant difference in responses to face images. We also tested these occluders on images of monkeys and humans, both separately and together, and found no significant differences. For this reason, we focus more on natural stimuli in our analyses.

The impact of facial image occlusion on the response characteristics of ITC and vlPFC neurons remains unexplored. In this study, we aimed to bridge this gap by systematically presenting facial images with varying degrees of occlusion, thereby elucidating

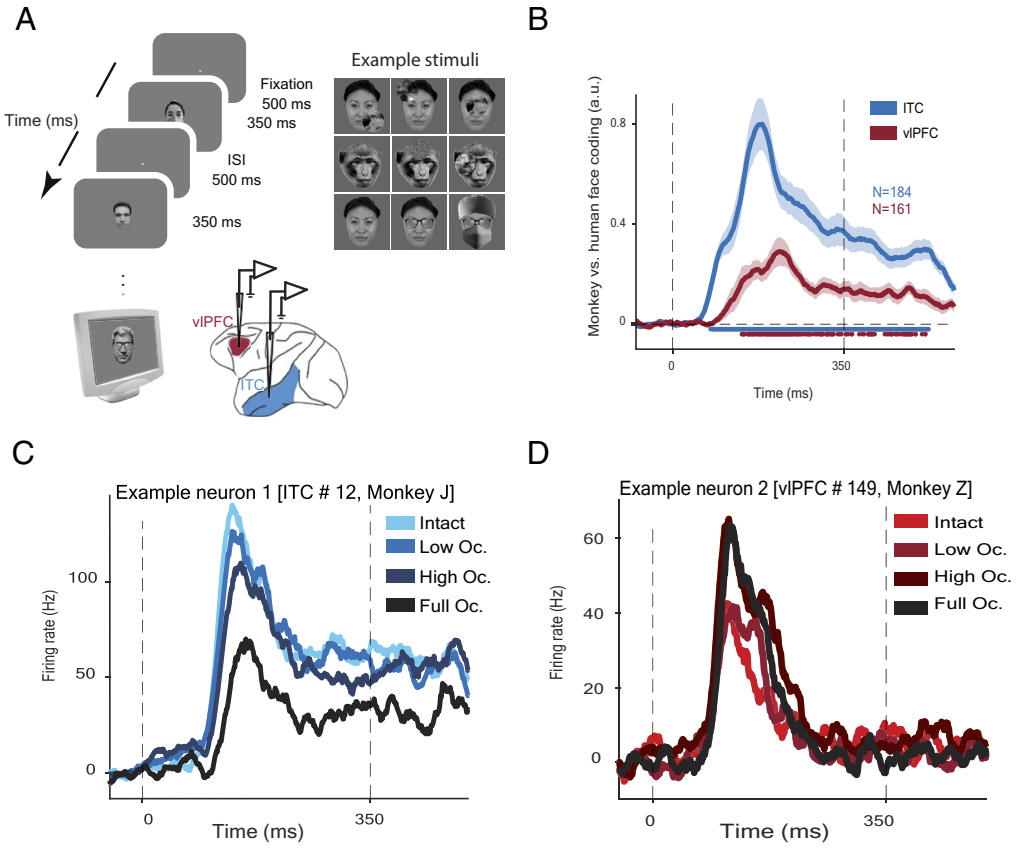

Fig. 1. The behavioral task involved processing category information. (*A*) In the passive task, monkeys fixated on a central point on the computer monitor while the stimulus was presented at that point. Simultaneously, spike activity and LFPs were recorded using a single electrode from the ITC and vlPFC regions of the monkey. Each stimulus condition was presented for 350 ms, followed by a 500 ms interstimulus interval (ISI). Example stimuli used in this study are shown. (*B*) In terms of category coding, ITC and vlPFC neurons exhibited category representations. Significance differences with baseline (−100 to 0 ms) were indicated by blue and red dots under the graph (error bars represent SEM; Wilcoxon rank-sum test; $P < 0.01$). (*C* and *D*) Sample PSTHs for neurons from the ITC and vlPFC at different occlusion levels are shown in (*C* and *D*), respectively.

the relationship between occlusion and neural responses in these cortical regions.

Different Representations for Occluded Faces in the ITC and vlPFC. The neural response of ITC neurons exhibits variability concerning distinct degrees of occlusion. The example neuron illustrated in Fig. 1*C* (for more example *SI Appendix*, Fig. S2*A*) exhibits a reduction in response as occlusion increases. Notably, intact stimuli elicit the highest firing rates, while those with full occlusion evoke the lowest firing rates. To find the relationship between neural responses and the level of stimulus occlusion (from intact to fully occluded faces in 4 levels), we used linear regression. The tuning curve illustrates how a neuron's firing rate changes in response to various levels of occlusion. A negative slope means the neuron's firing rate decreases as the level of occlusion increases, while for a positive slope, it is the opposite. The slope of the tuning curve demonstrates whether neurons prefer intact face stimuli (negative slope) or occluded ones (positive slope). It was observed that 71% of ITC neurons, specifically 131 out of 184, exhibited a negative slope, it was significantly more than 0.5 (binomial test, $P < 10^{-9}$). This indicates a preference for intact face images, classifying them as intact-sensitive neurons (ISNs). Conversely, 29% of neurons (53 out of 184; binomial test, $P < 10^{-9}$) displayed a positive slope, indicating a preference for responding to faces with occlusion, categorizing them as occlusion-sensitive neurons (OSNs) (Fig. 2 *A* and *B* and *SI Appendix*, Figs. S4 and S5 for both monkeys). The observed difference in the percentage of ITC neurons preferring intact stimuli between the two monkeys (Monkey J: 78%; Monkey Z: 53%) may be influenced by the nonuniform distribution of recorded neurons across anatomical regions, as shown in *SI Appendix*, Fig. S11 illustrating the anatomical recording locations in both the ITC and vlPFC. The results suggest that neurons within the ITC exhibit a higher degree of slope toward intact face stimuli (Fig. 2*D*; $m_{slope} = -0.19 \pm 0.016$, $P < 10^{-12}$). The representation of the average response over time for ISNs in the ITC reveals a statistically significant increase in their average response from 90 ms until the end of the stimulus display when comparing intact face stimuli to those with full occlusion (N = 131, $\mu_{intact} = 0.58 \pm 0.024$, $\mu_{full} = 0.03 \pm 0.005$, Wilcoxon signed-rank test, $P < 10^{-9}$; Fig. 2*C*).

Our study also identified neurons in the ITC with two distinct response phases (*SI Appendix*, Fig. S2*B*). During the first phase, many ITC neurons exhibited decreasing response with increased occlusion, while in the vlPFC region, neural activity increased proportionally with the level of occlusion in the presented facial stimuli (Fig. 1*D*; for more examples, see *SI Appendix*, Fig. S2*C*). The tuning curve slope for vlPFC neurons showed that over half of them had a positive slope at different occlusion levels (61%, 98/161, $P = 0.003$, Fig. 2 *E* and *F*), This suggests that vlPFC neurons can be categorized as OSNs (Fig. 2*H*; $m_{slope} = 0.05 \pm 0.017$, binomial test, $P < 10^{-5}$). Furthermore, the analysis of the average response in the peristimulus time histogram (PSTH) for OSNs in the vlPFC revealed a significant increase in neural response for fully occluded images compared to intact ones (N = 98, $\mu_{intact} = 0.10 \pm 0.021$, $\mu_{full} = 0.18 \pm 0.026$; Wilcoxon signed-rank test, $P < 10^{-16}$; Fig. 2*G* and *SI Appendix*, Fig. S4 for Monkey J and *SI Appendix*, Fig. S5 for Monkey Z).

The study's findings on artificial occluder placement show that different facial features hold varying importance to ITC neurons. When an occluder is placed over the left eye (location 4) or both eyes (location 5), neural responses differ significantly compared to other positions (Wilcoxon signed-rank test, $P < 0.05$) (*SI Appendix*, Fig. S13*A*). For human faces, placing the occluder at location 4 significantly affects neural responses (Wilcoxon signed-rank test, $P < 0.05$) (*SI Appendix*, Fig. S13*C*). In monkey faces, occluder placements at location 4 and location 5 lead to a significant decrease in ITC neuron activity compared to other positions, such as location 1 (*Top Left*), location 3 (Top Right), location 8 (*Bottom Left*), and location 9 (Bottom Right) (Wilcoxon signed-rank test, $P < 0.05$) (*SI Appendix*, Fig. S13*D*).

Representation of Occluded Faces in the Population of the ITC and PFC. To compare the similarity structure of neural response patterns to the similarity structure of experimental stimuli, we used representational dissimilarity matrix (RDM). An RDM reveals which differences between stimuli are highlighted and which are downplayed in the representation, effectively encapsulating, in an intuitive manner, the information content of the representation (24). Furthermore, to investigate the response pattern observed in ITC neurons, we employed the occluded models to indicate the incorporating level of occlusion. Each model represents a distinct degree of occlusion (Fig. 3*C*). The correlation between the occluded models and ITC ISN RDM was used to measure population coding (PC) of occlusion in neural circuits. We observed that the coding of occluded faces was robust in ITC neurons, as demonstrated in Fig. 3*G*. This finding indicates that even when parts of the faces were hidden, the neurons in the ITC were still able to process and represent the occluded faces. Notably, the highest ITC coding was observed in the neuronal responses of ITC ISN subpopulation for intact faces ($\mu_{intact} = 0.16 \pm 0.043$, $\mu_{full} = 0.01 \pm 0.045$; bootstrap test, $P = 0.04$; as depicted in Fig. 3*E*). Similarly, this approach was employed to examine occluded face coding in vlPFC OSN subpopulation. Consistent with tuning curve analyses, the vlPFC OSN subpopulation showed increased coding activity for more occluded faces, with the lowest activity observed for intact faces ($\mu_{intact} = -0.02 \pm 0.044$, $\mu_{full} = 0.10 \pm 0.057$; bootstrap test, $P = 0.06$ Fig. 3*H*). These results demonstrate that consistent with individual neurons, different levels of occluded stimuli are represented on the activities of population in both the ITC and vlPFC.

Dissociation of Occlusion from Identity Processing in the ITC and vlPFC. To distinguish the effects of occlusion processing from identity processing, we employed GLM analysis. Additionally, we mitigated the impact of confounding factors, including luminance, identity information, and the first and second principal components obtained through principal component analysis (PCA) of the stimuli (refer to the Materials and Methods section). This approach allowed us to dissociate the specific impact of occlusion level on the outcome, regardless of the influence of identity or other features. As depicted in Fig. 4*A*, the contribution of occlusion processing of the ITC decreases with the increase of occlusion level (in ISNs; compared to the baseline, $\mu_{IT} = -3.61 \pm 0.749$, Wilcoxon signed-rank test; $P < 10^{-11}$). This analysis shows that as more of the face is covered, the response of ITC neurons decreases. This reduction indicates that ITC neurons are specifically tuned to process complete facial features and their response diminishes as the face becomes more occluded. In contrast, the response of vlPFC neurons increases with occlusion (in OSNs; $\mu_{vlPFC} = 1 \pm 0.561$, vs. baseline, Wilcoxon signed-rank test; $P = 0.002$). The responses of both groups of ISNs and OSNs in the ITC and vlPFC are depicted in *SI Appendix*, Fig. S6. This finding suggests that the vlPFC neurons' responses become more pronounced as the level of occlusion increases. This indicates that the vlPFC neurons are specifically influenced by increasing levels of occlusion, even after accounting for potential confounding variables, including luminance and identity information.

Examining the temporal dynamics in the GLM shown in Fig. 4, the ITC figure displays two clear phases. The first phase occurs around

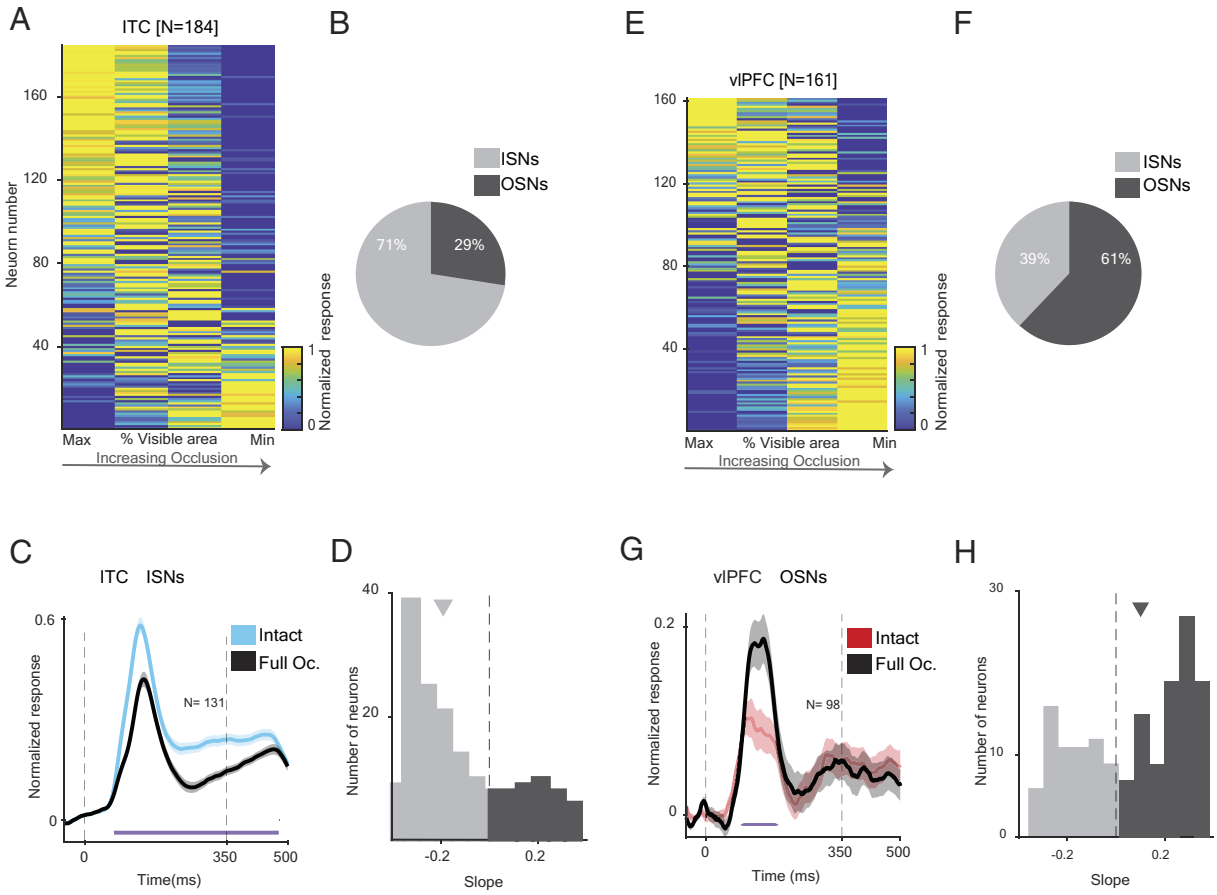

Fig. 2. Population responses in ITC and vlPFC neurons. (*A*) Average responses (0 to 350 ms) to occlusion were normalized (columns). The visible area is ranked along the abscissa, so each column may show a different amount of occlusion for each neuron. From left to right, the level of occlusion increases while the visible area decreases. Neurons were studied with four levels of occlusion (184 ITC neurons and 161 vlPFC neurons). Responses were normalized to each neuron's highest response. (*B*) Most ITC neurons responded strongly (yellow) to low-level occluded faces and weakly (blue) to higher levels of occlusion. (*C*) Most vlPFC neurons responded strongly (yellow) to occluded faces and less strongly (blue) to low-level occluded faces. Specifically, 131/184 (71%) of ITC neurons and 63/161 (39%) of vlPFC neurons responded to intact faces. The responses of ITC and vlPFC neurons to occluded faces were 29% (53/184) and 61% (98/161), respectively. (*D*) Average responses normalized using data from ISN and OSN vlPFC at intact and full occlusion levels. The purple dots indicate significant differences between responses to intact and fully occluded images (error bars represent SEM; Wilcoxon signed-rank test; $P < 0.05$). (*E*) The responses in panels A and D were fitted using the distribution of linear regression slopes. (*F*) Negative slopes were present in the majority of ITC neurons (131/184), indicating stronger responses to intact stimuli; the median slope was −0.19. (*G*) In contrast, positive slopes were observed for the majority of vlPFC neurons (98/161), indicating higher responses to occluded stimuli; the median slope was 0.05. (*H*) Overall, these findings highlight the differential neural responses in the ITC and vlPFC to various levels of occlusion.

122 ms (mean first phase = 122 ± 2.4 ms), followed by the second phase around 260 ms (mean second phase = 260 ± 4.3 ms) (Fig. 4 *B*, *Top*). In the vlPFC graph, a single phase is observed at approximately 150 ms (m = 150 ± 8.4 ms) (Fig. 4 *B*, *Down*), which occurs between the first and second phases seen in the ITC. This temporal relationship suggests a potential interaction and coordination between the neural activity in the vlPFC and the two phases observed in the ITC.

Decoding of Occluded Face Representation in the ITC and vlPFC. To explore the decrease in ITC neuron response and the increase in vlPFC neuron response to occluded images, we studied the decoding of male and female images at various occlusion levels. Does the decoding accuracy between male and female classes in the ITC and vlPFC remain consistent across levels of occlusions? If the decoding accuracy remains consistent across all occlusion levels in both areas, it suggests that occlusion is not a factor in this category. Otherwise, it indicates that ITC and vlPFC neurons encode occlusion.

We labeled our stimuli as male and female to assess the decoding of neuronal populations at different occlusion levels in both regions. We used a linear support vector machine (SVM) to analyze the decoding accuracy between male and female faces at each occlusion level individually. We measured the decoding of two phases in ITC neuronal responses separately. In Fig. 5*A*, we illustrate the decoding of the initial phase of ITC neurons. Without occlusion, the decoding accuracy is higher compared to fully occluded images in the ITC region for distinguishing between male and female faces. However, as the occlusion level rises, the decoding accuracy in the ITC region gradually declines (μ_{intact} = 90.7% ± 9.9; μ_{full} = 43% ± 15.6, bootstrap test, P = 0.03). This suggests that the ability to accurately decode gender information in the ITC region is affected by the presence of occlusion. On the other hand, in the vlPFC, the decoding accuracy for intact face images was low and similar to chance levels. However, with an increase in occlusion, the decoding accuracy showed improvement (μ_{intact} = 50.2% ± 14.2 vs. μ_{full} = 88.5% ± 11.6). Decoding between male and female classes showed significant differences when comparing intact stimuli to fully occluded images in both regions (bootstrap test, p_{IT} = 0.049, p_{vlPFC} = 0.036). Fig. 5*B* illustrates the difference in decoding for male and female faces between the vlPFC and ITC. The plot indicates that as the level of occlusion in the stimuli increases, the accuracy of decoding in the vlPFC region increases, while it decreases in the ITC region ($\Delta\mu_{intact}$ = −36.4% ± 14.4, $\Delta\mu_{full}$ = 37% ± 12., bootstrap test, P = 0.03). These findings indicate that the ITC area specializes in processing images without occlusion, while the vlPFC area is involved in processing information related to occlusion. During the

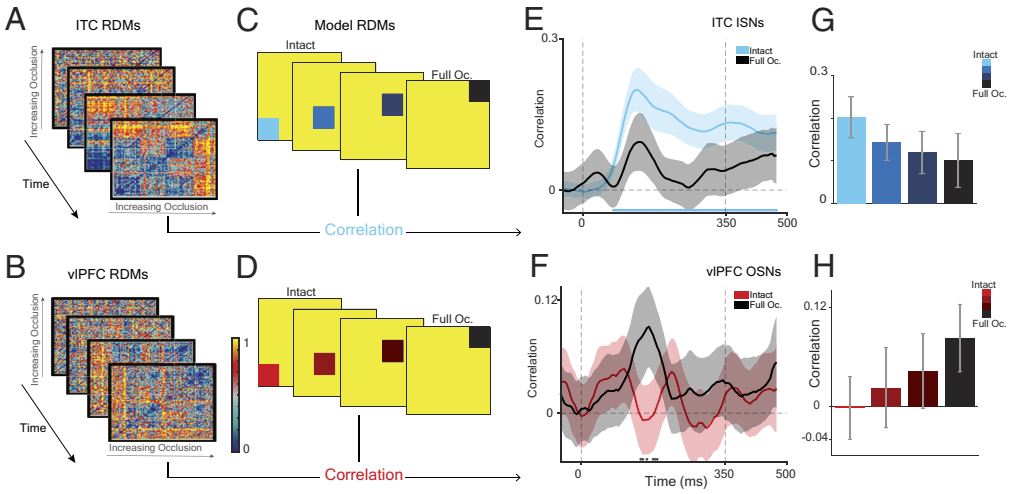

Fig. 3. Population coding using RSA. (*A* and *B*) The neural representational dissimilarity matrices (RDMs) were calculated in a time window of 30 ms for each area (ITC in part a; vlPFC in part c) covering all neurons (see the *Materials and Methods*) section. (*C* and *D*) The model is constructed to simulate the representation and processing of information in the brain. These predicted patterns are then compared to the actual patterns of neural activity measured experimentally. (*E* and *F*) RSA yields intriguing results by contrasting the actual patterns of neural activity (represented by RDMs) over time for the ITC and vlPFC regions with the predicted patterns generated by the model. In the ITC region, there is a greater degree of similarity between the neural activity patterns and the intact model compared to the fully occluded model. Conversely, in the vlPFC region, there is a greater similarity between the neural activity patterns and the fully occluded model compared to the intact model. (*G* and *H*) Furthermore, as the level of occlusion increases, the bar plot demonstrates a decrease in the correlation of RSA for the ITC region. In contrast, for the vlPFC region, the correlation of RSA increases with higher levels of occlusion. The error bars, representing the SE, are depicted based on 500 bootstrap iterations. The lines beneath the curves on the e and f indicate significance with zero (bootstrap test, $P < 0.05$).

second phase of decoding occlusion levels in the ITC, there was a clear difference compared to the first phase. Specifically, in the second phase, the accuracy of decoding between images of male and female faces was higher, particularly for high and full levels of occlusion (Decoding ITC Phase 2–Phase 1; μ_{intact} = 7.5% ± 10.6, μ_{low} = 5% ± 13.1, μ_{high} = 19.4% ± 21.5, μ_{full} = 33% ± 19.3). This indicates that the second phase of the ITC provides better decoding accuracy compared to the first peak, particularly for more occluded images. However, the difference in decoding accuracy between intact images and fully occluded images is not statistically significant in the second phase of the ITC (Bootstrap test, P = 0.06), suggesting that the accuracy for fully occluded images increases and approaches that of intact images. This increase indicates that, during the second phase of neuronal response decoding, occluded images are decoded approximately 30% more accurately compared to the first phase decoding by the same neurons. The difference between the vlPFC and the first phase of the ITC for intact images is around 36% ($\Delta_{vlPFC\text{-}ITC1}$; μ_{intact} = −36.4% ± 14.4), increasing to about 43% ($\Delta_{vlPFC\text{-}ITC2}$; μ_{intact} = −43.9% ± 14.4), with the second phase of the ITC. There is no significant distinction in intact images between the first and second phases of the ITC. However, for full occluded images, the difference between the vlPFC and the first and second phases of the ITC is 37% ($\Delta_{vlPFC\text{-}ITC1}$; μ_{full} = 37% ± 13, P = 0.03), and 6% ($\Delta_{vlPFC\text{-}ITC2}$; μ_{full} = 6.8% ± 13, P = 0.03), respectively. This indicates that during the second phase of the ITC, decoding of occluded images is more pronounced compared to the first phase and is similar to vlPFC decoding. Fig. 5*B* shows the differences in decoding between the vlPFC and the first phase of the ITC across all levels of occlusion. A value below zero indicates that the ITC outperforms the vlPFC in decoding, while a value above zero indicates better decoding by the vlPFC. When subtracting the decoding values for the fully occluded level, the difference between the vlPFC and the first phase of the ITC is more pronounced, while the difference for the second phase is smaller. This suggests that the second phase of ITC decoding is more similar to that of the vlPFC ($\Delta_{vlPFC\text{-}ITC1}$, P = 0.03, $\Delta_{vlPFC\text{-}ITC2}$, P = 0.03).

Comparisons of decoding accuracy between intact and low occlusion levels in the ITC revealed a significant difference from the shuffled data (intact vs. low, $P < 10^{-3}$). In contrast, decoding accuracies for high and full occlusion levels did not exhibit significant differences from the shuffled data. In the PFC region, all occlusion levels except for the intact condition showed significant deviations from the shuffled data, with low, high, and full occlusion levels each differing significantly ($P < 0.01$).

The Influence of the vlPFC on Shaping ITC Representation. From the findings in the earlier figures, it was evident that the processing of the initial and second phases in ITC neurons differs when dealing with occluded images. The vlPFC or higher regions likely contribute different information during the second phase of ITC neuron response to enhance the processing of occluded images. To explore this further, we conducted a Granger causality analysis on the RDMs to investigate whether the second ITC peak receives information from the vlPFC. The RDMs enable us to compare the representations of the ITC and vlPFC. By assessing how much the RDMs of one region can predict or "cause" the RDMs of another brain region, we calculate the influential relation between the two areas (24). This analysis helps to uncover the directional flow of information and the influence of one brain area on another. Statistically significant information transfer curves are observed between 95 and 130 ms ($\mu_{ITC\rightarrow vlPFC}$ = 0.009 ± 0.002), 145 to 220 ms ($\mu_{ITC\rightarrow vlPFC}$ = 0.033 ± 0.004), and 305 to 320 ms ($\mu_{ITC\rightarrow vlPFC}$ = 0.010 ± 0.003) from the ITC to the vlPFC when compared to baseline activity (bootstrap test, $P < 0.05$) (Fig. 6*B*). Data transfer from the ITC to the vlPFC begins around 95 ms, reaching its peak between 145 and 220 ms (m_{Peak} = 181 ± 1 ms). This timeframe follows the peak time of the initial phase of ITC neuron responses ($m_{first\ P}$ = 122 ± 2.4 ms). This time frame aligns with the processing of occluded faces in the vlPFC, as demonstrated in the previous figure (Fig. 4). This suggests that the vlPFC receives necessary information from the ITC. The information transfer curve from the vlPFC to the ITC shows a significant difference from the baseline during two-time intervals: 200 to 300 ms ($\mu_{vlPFC\rightarrow ITC}$ = 0.017 ± 0.003), and 375 to 425 ms ($\mu_{vlPFC\rightarrow ITC}$ = 0.014 ± 0.002; bootstrap test, $P < 0.05$). The second peak observed in Fig. 6*B* indicates a significant flow of information from the vlPFC to the ITC (The first red peak),

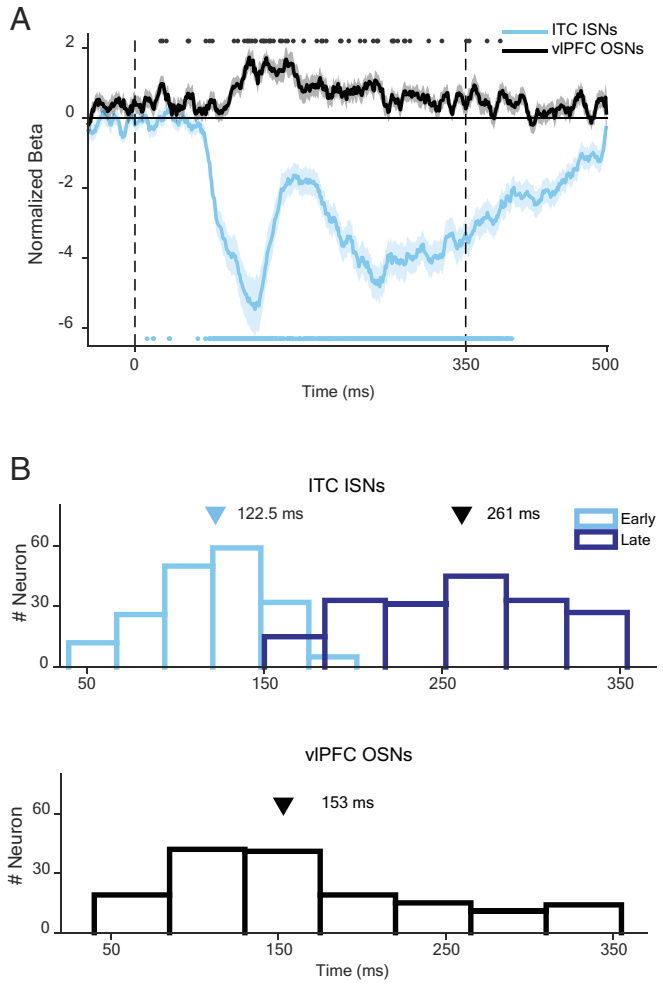

Fig. 4. Dissociation of occlusion compared to face identity representation in the ITC and vlPFC. (*A*) Displays the contribution of occlusion level extracted from the GLM analysis over time for the ITC (blue) and vlPFC (black) regions. The black and blue dots positioned above and below the figure indicate the time points at which there is a significant difference compared to the baseline (the shadow represents the SEM, calculated over the number of neurons; Wilcoxon signed-rank test; $P < 0.05$). (*B*) The histogram illustrates the peak times for part a. Specifically, the ITC region exhibits two distinct phases, with peak times occurring at approximately 122 and 261 ms, respectively. On the other hand, the vlPFC region demonstrates a single peak at around 153 ms.

representing the neural correlation of feedback connection of PFC signals into the ventral stream ($\mu_{vlPFC \to ITC} = 0.017 \pm 0.003$; bootstrap test, $P < 0.05$). Notably, the figure demonstrates that the time needed for transferring information related to occlusion from the vlPFC to the ITC falls within the interval of 200 to 300 ms. This timeframe aligns with the second processing phase in the ITC, as identified in prior analyses ($m_{second\ P} = 260 \pm 4$ ms). The transfer of information from the vlPFC to the ITC is believed to shape the representation of occluded stimuli and aid in resolving the problem of occlusion and challenging stimuli in the ventral visual stream. In other words, the vlPFC appears to play a role in providing feedback to the ITC, which helps in processing and integrating occluded facial features to resolve the issue of occlusion.

The ITC Has Two Distinct Neural Mechanisms for Processing Occluded Faces in the First and Second Phases. To uncover neural mechanisms over time in the ITC and vlPFC, we use time–time decoding analysis. Time–time decoding analysis in the ITC and vlPFC allows us to understand the temporal dynamics of neural activity in these brain regions. This analysis allows the identification of cortical sources that drive visual processing and enables us to distinguish different processing strategies within a single cortical area. Additionally, examining how the decoding accuracy changes over time provides evidence for understanding the neural mechanisms involved in processing occluded faces. The time–time decoding analysis was conducted in two ways to evaluate decoding performance in different scenarios. In the first analysis, we used labels for intact and low occlusion (IL occlusion), training at one time and testing at another time. In the second analysis, the labels were intact and full occlusion (IF occlusion). We observed two distinct phases of decoding performance (Fig. 7 *A* and *B*). The first phase occurred between 70 and 200 ms, while the second phase occurred after 200 ms (Fig. 8 illustrates two distinct zones for the ITC). The decoding performance in the ITC region revealed different patterns between the IL occlusion and the IF occlusion. The second phase of decoding in the IF occlusion condition demonstrated significantly higher performance compared to the second phase of the IL occlusion condition ($\mu_{IF\ p2} = 37.8\% \pm 1.8$, $\mu_{IL\ p2} = 32.5\% \pm 2.4$; Wilcoxon signed-rank test, $P = 10^{-36}$). This observation confirms the two distinct phases in the ITC and indicates a higher contribution of the late phase in the processing of occluded faces as challenging stimuli.

Within the specific time window of 125 to 200 ms in the vlPFC region, there is a single processing period, consistent with the unimodal observed in the representation of occluded faces in this area. Furthermore, we demonstrate a clear difference between the IF occlusion and IL occlusion conditions, confirming increased engagement of the vlPFC in facial processing with greater occlusion ($\mu_{IF} = 30.7\% \pm 2.5$, $\mu_{IL} = 37\% \pm 1.4$; Wilcoxon signed-rank test, $P < 10^{-5}$, Fig. 7 *C* and *D*). The results illustrating the difference between the IF occlusion and IL occlusion conditions (IF-IL) in the ITC and vlPFC regions are presented in *SI Appendix*, Fig. S7.

The distinctive decoding pattern in the ITC time–time plot confirms the dissociation of the first and second phases for processing different aspects of input stimuli. In the first phase, the ITC is more engaged in the detection of stimuli, while in the second phase, influenced by vlPFC feedback, it is involved in resolving the occluded aspects of stimuli.

Enhanced Synchronization between the ITC and vlPFC during Occlusion Face Processing. We observed that information related to occluded stimuli is transferred from the vlPFC to the ITC within the time interval of 130 to 200 ms. Consequently, the feedback connection suggests greater coordination for stimuli with higher occlusion than for images without occlusion during this time. The phase locking value (PLV) analysis is a method used to measure the degree of synchronization or coherence between two brain regions. This analysis is valuable for understanding the functional connectivity and communication between different brain areas during various cognitive processes. Empirical investigations have consistently demonstrated that heightened alpha-beta synchrony between brain areas is indicative of the involvement of Top–Down processes (25–27). This synchronization is believed to facilitate the integration of information across brain regions, thereby promoting effective communication and coordination among them (25–27).

Using PLV analysis, we quantified the degree of synchrony between the ITC and vlPFC during the processing of full occlusion faces compared to intact faces. The PLVs within the alpha-beta frequency band for both intact and full occluded images ranged between 7 and 17 Hz (Fig. 8*A* and *SI Appendix*, Fig. S8 provides additional examples for both monkeys). The results illustrating the difference between these two conditions revealed a higher degree of locking value for full occluded images compared to intact images ($\mu_{intact} = 2.88 \pm 0.332$, $\mu_{full} = 3.88 \pm 0.623$, $P < 10^{-11}$ Similar in both, every distinction from the baseline). Furthermore, Fig. 8*B* demonstrates that the locking phase of

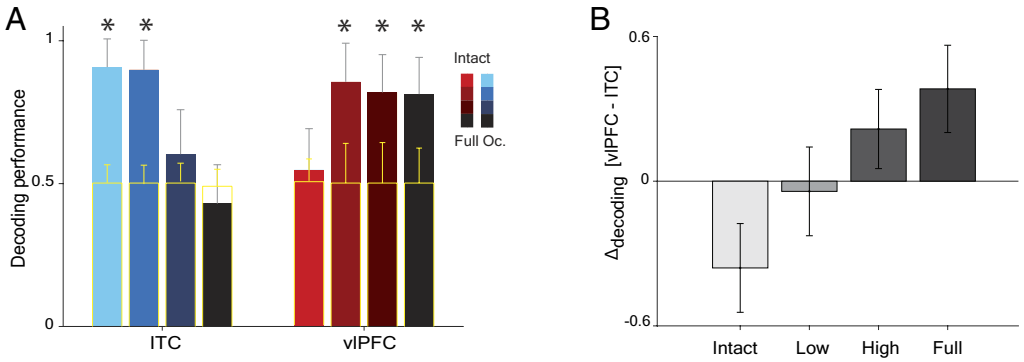

Fig. 5. Population decoding using SVM classification. (*A*) The bar plot illustrates the decoding performance of gender (male and female) across different levels of occlusion. It is evident that the decoding of gender in the ITC region is higher for intact images, while the decoding of gender in the vlPFC region is more pronounced for occluded images. (*B*) The bar chart depicts the difference in decoding accuracy between the vlPFC and ITC (vlPFC-ITC) across different levels of occlusion (the error bars represent the SE). This plot exclusively displays data from the first phase of the ITC. The yellow bar plots represent the shuffled data. An asterisk on each bar denotes a significant difference compared to the shuffled data.

full occluded images exhibited a significantly higher value between the time intervals of 150 and 195 ms compared to the locking phase of intact images (μ_{intact} = 2.88 ± 0.332, μ_{full} = 3.88 ± 0.623; *SI Appendix*, Fig. S9; Wilcoxon signed-rank test, $P < 0.01$). As expected, the time period during which phase locking between different occlusion levels is significant (150 to 195 ms) aligns with the time window of information transfer from the vlPFC to the ITC in the Granger causality analysis (130 to 200 ms), as well as with the time window of time–time decoding (125 to 200 ms).

These findings provide evidence of a consistent upward trend in the locking value between the ITC and vlPFC as the levels of occlusion increase (μ_{intact} = 2.88 ± 0.332, μ_{low} = 3.29 ± 0.478, μ_{high} = 3.65 ± 0.506, μ_{full} = 3.88 ± 0.623; *SI Appendix*, Fig. S9). The examination of the data depicted in Fig. 8*C* reveals a higher PLV for images with occlusion compared to images without occlusion (36/58, $P = 0.03$; Wilcoxon signed-rank test intact vs. full, $P < 0.01$; intact-full $\mu = -0.89 \pm 0.366$). This suggests increased functional connectivity and synchronization between frontotemporal networks during occluded stimuli processing, potentially facilitating the integration and interpretation of visual information.

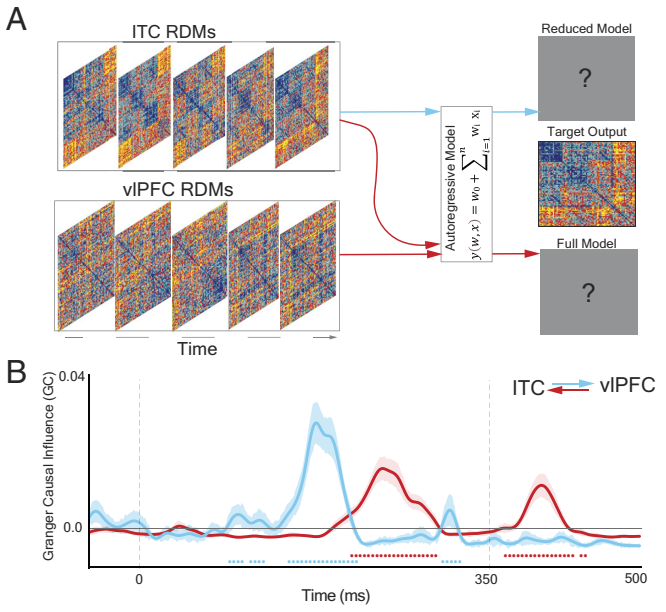

Fig. 6. Neural information flow in the ITC and vlPFC. (*A*) The application of an autoregressive model on RDMs involves using these representations as input to predict future ones, assuming that the current state of the system can be predicted based on its past states. Granger causality analysis can be applied to assess whether RDMs in one brain region can predict or "cause" RDMs in another, revealing the directional flow of information between regions. This analysis aids in understanding how neural representations in one region may influence or drive representations in another over time. (*B*) The plot of Granger causality on RDMs illustrates the direction of information flow between the ITC and vlPFC regions. The blue curve shows information flowing from the ITC to the vlPFC during time intervals 95 to 130, 145 to 220, and 305 to 320 ms, and this is significantly different from the baseline.

Occlusion Increases Microsaccade Activity but Does Not Affect Pupil Size. Microsaccades are small, involuntary eye movements that occur even when the gaze is fixed. These movements are crucial for maintaining visual acuity and compensating for the sensory fading of the retinal image. Research has shown that microsaccades play a role in visual processing even in passive viewing conditions, making them a valuable metric in such studies. Research shows that microsaccades, even during passive viewing, offer important insights into how we process and stabilize visual information, making them a valid behavior to study in passive paradigms (28). We analyzed microsaccade rates for intact and occluded face images. As shown in Fig. 9*A*, the rates are similar for both types of images until the end of the first phase of ITC neuron responses. However, starting from the second phase, there is a significant difference in microsaccade rates between intact and occluded images (Wilcoxon signed-rank test, $P < 0.05$).

Pupil size is affected by stimulus properties such as size, contrast, and spatial frequency, with larger stimuli generally causing greater constriction, independent of luminance (29, 30). Increased cognitive load leads to larger pupil sizes, making it a reliable measure of cognitive effort (31). Our results, shown in Fig. 9*B*, reveal that pupil size remained consistent for both intact and fully occluded stimuli throughout the observation period. There were no significant differences in pupil size between the two conditions, indicating that the cognitive and perceptual demands were similar for both intact and occluded stimuli. To ensure that brain state did not influence the processing of occluded images, we conducted an analysis. We sorted the trials for both intact and occluded face images based on pupil size. We divided the trials into two categories based on pupil size: small and large. For each category, we calculated the PLV separately for intact and occluded face stimuli across the relevant brain regions. The results showed that, regardless of pupil size, the PLV for occluded images was consistently higher than for intact images (*SI Appendix*, Fig. S10). This indicates that the difference in neural responses is related to how the brain processes occlusion, independent of brain state or arousal levels.

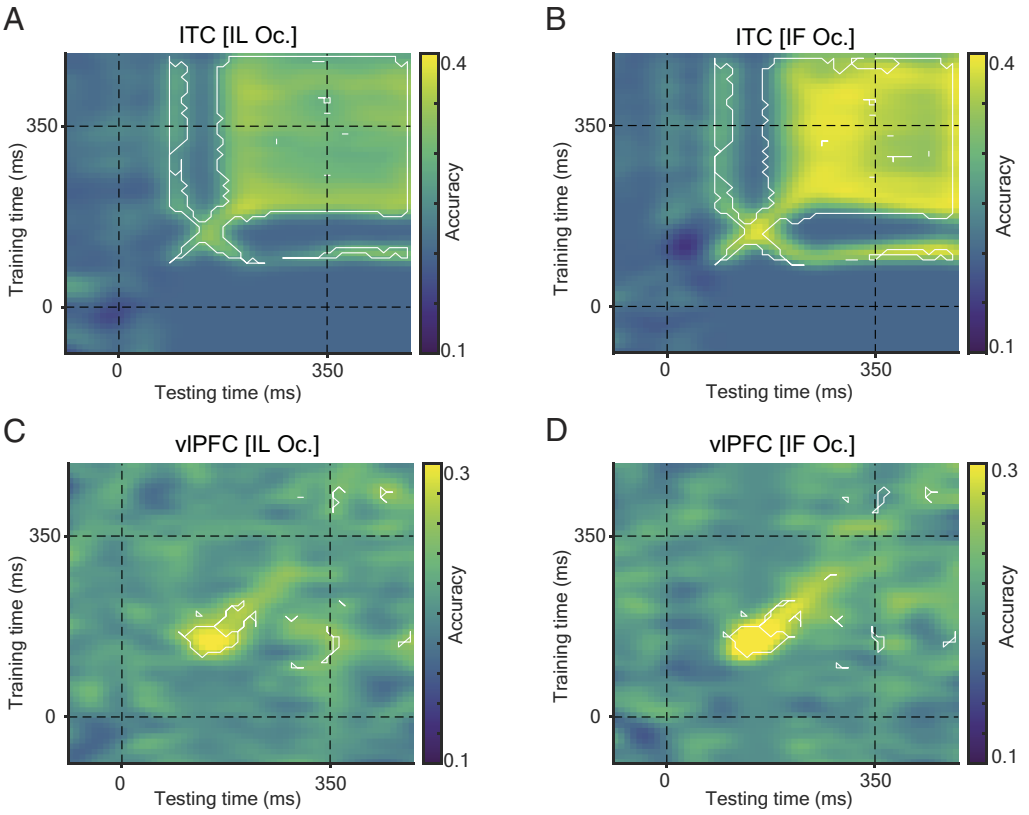

Fig. 7. Comparative analysis of time–time decoding in the ITC and vlPFC. (*A*) The temporal dynamics of decoding accuracy for faces with IL occlusion in the ITC region are revealed by the time–time decoding analysis. Two distinct phases of decoding are observed, with the first phase occurring between 70 and 200 ms and the second phase occurring after 200 ms. (*B*) Similarly, in the time–time decoding analysis for faces with IF occlusion in the ITC region, two distinct phases are observed. However, the decoding performance accuracy is higher compared to faces with IL occlusion. (*C* and *D*) In the vlPFC region, the time–time decoding analysis demonstrates that the decoding accuracy reaches its peak between 125 and 200 ms, regardless of the level of occlusion. Notably, there is a significant difference in the decoding accuracy between faces with IF occlusion and faces with IL occlusion in the vlPFC region bootstrap test ($P < 0.05$).

Discussion

The main goal of this study was to investigate how the brain, particularly the ITC, responds to partially occluded faces and the role of the vlPFC in this process. In our initial investigation, we observed reduced neural responses in the ITC to varying levels of occlusion in facial stimuli, with some neurons exhibiting a two-phase response (*SI Appendix*, Fig. S2). Additionally, our analysis uncovered the involvement of the second phase of the ITC in processing occluded stimuli. We also found the role of the vlPFC in processing occluded facial stimuli, occurring before the second phase of ITC activity. Our study revealed that as the level of occlusion in the visual stimuli increased, there was a greater level of coordination observed between the ITC and vlPFC regions of the brain. We also identified that the neural mechanism in the second stage of the ITC response, specifically after 180 ms, was found to be involved in processing facial stimuli that were occluded or partially occluded. We noticed that the vlPFC has an important function in representing the activity of the second phase of neurons in the ITC when processing faces that are occluded or partially obscured. The vlPFC provides essential information to the ITC through feedback. Our results demonstrate the separation of occlusion processing from identity processing and emphasize the significant contribution of the vlPFC in representing the second phase of ITC neurons for occluded faces.

Additionally, the results from the artificial occluders confirmed that the eyes are crucial for facial recognition, consistent with Issa and DiCarlo (13). We also found that occlusion has a greater impact on conspecific images compared to images of other species, which is consistent with previous studies (32, 33). This comparison is shown in *SI Appendix*, Fig. S13 *C* and *D*.

The ITC Processes Face Identities, while the vlPFC Deals with the Challenge of Processing Occluded Face Stimuli. Behavioral studies have demonstrated that occluded stimuli are rapidly and completely represented (34, 35), and this ability has been observed even in infants as well (36–40). Because the information from the covered parts of occluded stimuli is not projected onto the retina, it has been observed that the response of neurons to occluded stimuli can differ from that to complete stimuli (12, 17). Our findings revealed that the response of a majority of neurons in the ITC region (71%) decreases when presented with occluded stimuli (ISNs), while only a small percentage (29%) of the neurons in this region increase their response (OSNs). Various studies present conflicting findings regarding neural responses to occluded and intact stimuli. Some indicate that neuron response to intact stimuli is greater than to occluded stimuli (11, 12, 17, 41–43), while others suggest the opposite (10, 42, 44, 45), and some studies report equivalent responses to both intact and occluded stimuli (40, 42, 46–48). In the imaging study, it was revealed that the selective-face area is also dedicated in processing occluded face stimuli (46). This aspect was taken into account in our study, where we recorded face-selective neurons in the ITC to explore the impact of facial occlusion. Additionally, it is noted that low-level visual areas process simple occluded stimuli, while more complex occluded stimuli are processed in higher vision areas (40). Numerous studies have shown that the brain contains specific areas and circuits dedicated to processing facial stimuli (6, 22, 46, 49–53), as well as other types of stimuli (54–56). Discrepancies in occlusion study results may arise from factors such as recording from selective or nonselective neurons, using static or dynamic occlusion stimuli, employing two-dimensional or three-dimensional occlusion stimuli, variations in experimental paradigms, and differences in the duration of stimulus presentation. Our results indicate that the response of face-selective neurons decreases as more facial features are covered. This finding aligns with studies that have recorded the selectivity and preference of neurons for the stimulus (11–13).

The representation of facial stimuli with varying levels of occlusion in the vlPFC revealed that many neurons in this area exhibit a stronger response to occluded face stimuli, aligning with previous study by

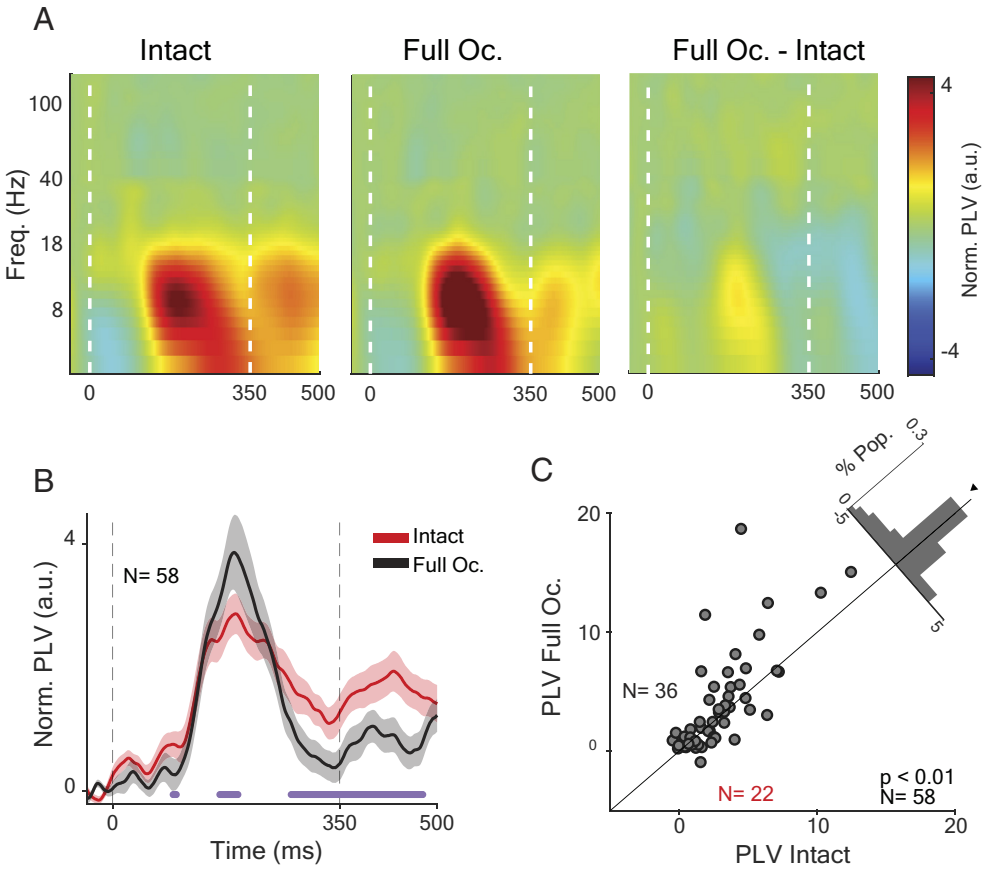

Fig. 8. Uncovering the influence of occlusion on neural synchronization. (*A*) The PLV between the ITC and vlPFC regions is shown for intact stimuli and full occlusion. Prior to the second phase of the ITC, there is a high PLV observed in the 7 to 17 Hz frequency range. The difference heat map clearly indicates a greater degree of locking in the presence of occlusion. (*B*) In the analysis of PLV for the frequency range of 7 to 17 Hz over time, a significant difference is observed between the intact and full occlusion conditions within the time window of 155 to 195 ms. (*C*) In the scatter plot, it is evident that a higher proportion of the pairs for PLV show greater PLVs for full occlusion compared to intact images (62%), indicating a significant difference (Wilcoxon signed-rank test, with $P < 0.01$). The median value of −0.29 for this distribution indicates that the majority of the PLVs are skewed toward the side of full occlusion.

Fyall et al. (17). There has not been any research exploring occluded face representation in this vlPFC region. The response of many vlPFC neurons increases as more parts of the face are covered, a pattern distinct from the response of neurons in the visual pathway.

Two factors can contribute to the enhancement of vlPFC response as the extent of occlusion increases. First, neurons in the vlPFC area respond to the occluders rather than the face itself, leading to an increased response with more occluder content. Second, as the level of face occlusion rises, processing these images becomes more challenging, leading to increased engagement of vlPFC neurons. Consistent with previous studies, our observations confirm the second hypothesis (17, 42). Therefore, the vlPFC is involved in occluder processing as a center for resolving challenging stimuli (15). As the level of occlusion increases, the challenge on stimuli also increases, leading to higher engagement or activity of the vlPFC.

In our design, one occluder stimulus contains both identity and occlusion information simultaneously. While higher-order visual areas are known for representing object-specific information, such as the category or identity of occluded objects (43), distinguishing neurons' responses to different occlusion levels from the stimuli's identity remains unclear. To address this, we employed a generalized linear model (GLM) to measure the contribution of various factors, including different levels of occlusion, basic visual features (i.e., PC1 and PC2), and identities of stimuli. The GLM enables us to dissociate the contribution of occlusion levels from identity representation and simultaneously control for the effects of visual confounding factors.

The First and Second Phases of ITC Neurons Exhibit Distinct Neural Mechanisms. In the temporal dynamics of many ITC neurons, we observed two response phases in both single-neuron (Fig. 2*S*) and population-level analyses (Figs. 4 and 5). In this study, our results show that the first and second phases of the response of ITC neurons in the processing of face stimuli differ. Our results show that the second phase of the response of these ITC neurons is involved in the processing of occluded face stimuli, which is consistent with previous studies on the processing of challenging images in the second phase of the neurons' response (12, 16). Our results indicated that the first phase response of ITC neurons occurs between 90 and 150 ms, while the second phase response occurs after 180 ms. Studies on occluded stimuli have demonstrated that these stimuli are processed with a longer delay than nonoccluded images (11, 16, 57, 58). The temporal dynamics of the face and fully occluded face representation reveal distinct neural mechanisms in the early and late phases of response. The time–time decoding matrices show that the decoding accuracy for occluded faces in the second phase in the ITC was higher than for intact faces. This suggests that the information content in the second phase differs from that in the first phase of the occlusion condition and is likely received from other areas. These results are consistent with previous studies, showing that the second phase of the response in the ITC to occluded stimuli not only receives information from the feedforward flow but also gets input from other areas (40).

The Feedback from the vlPFC Can Modulate the Second Phase of ITC Activity in Response to Occluded Faces. Our findings showed that the second phase in the ITC gathers more information from occluded stimuli than what the feedforward route offers. Theoretical studies show higher prediction accuracy of ITC neural response in the first phase compared to the second phase, indicating the absence of feedback information in the first peak and underscoring the role and significance of recurrent and feedback circuits in the second phase (56–59). While various downstream areas, including the vlPFC, perirhinal cortex, amygdala, and striatum, can participate in information transfer through feedback or recurrent pathways (59, 60), previous research suggests that the vlPFC plays a more substantial role (16, 17, 61). Anatomical

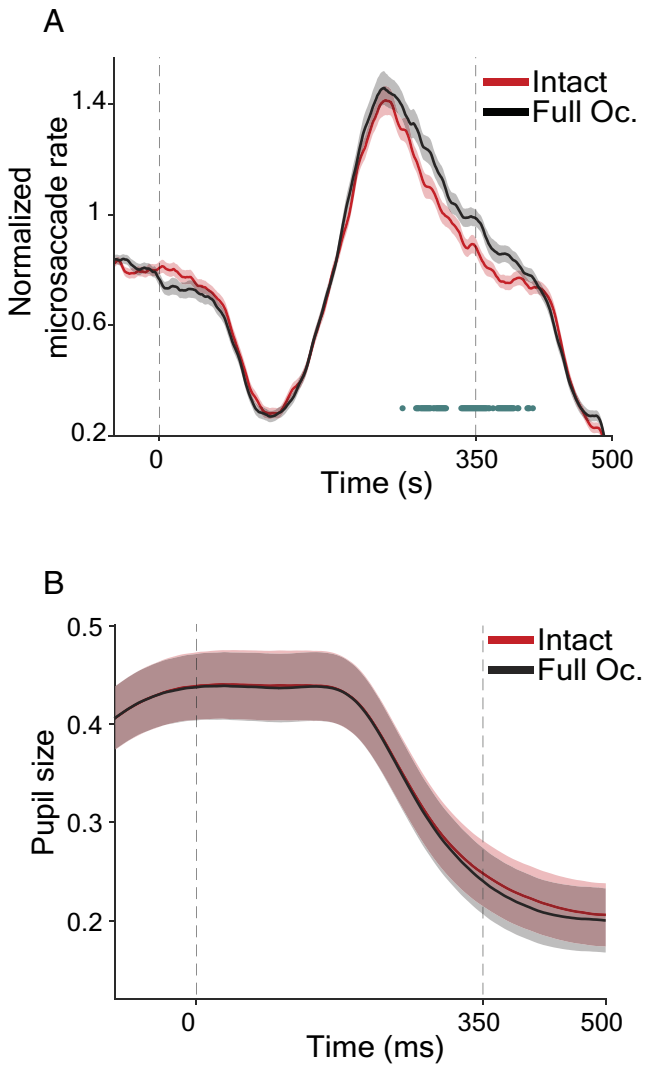

Fig. 9. Microsaccade and pupil size responses. (*A*) Microsaccades for intact and fully occluded conditions are similar until 250 ms. After 250 ms, microsaccades increase more for the fully occluded faces compared to the intact stimulus. (*B*) Pupil size for intact and fully occluded conditions is similar throughout the entire time period, with no significant differences between them. The blue dots show the significant times between two intact and full occluded image responses (the error bar represents SEM; Wilcoxon sign rank test; $P < 0.05$).

studies have demonstrated a direct connection between the vlPFC and visual areas such as the ITC (62, 63).

Employing Granger Causality Analysis allowed us to demonstrate the flow of information processing originating from the vlPFC, with the second phase of ITC processing receiving information from PFC. Consistently, the temporal dynamics of the response of vlPFC neurons (130 to 200 ms) to occluded faces preceded the processing of the second phase of neurons (180 to 300 ms) in the ITC. Therefore, our findings indicated that the second phase of the ITC is responsible for processing stimuli with occlusion.

Pharmacologically deactivating the vlPFC impairs its role in processing challenging stimuli in the second phase of the ITC (16). Additionally, the longer reaction times for challenging stimuli compared to nonchallenging stimuli (23) suggest the importance of receiving information from the vlPFC for correctly perceiving occluded stimuli. Our observations offer a neural mechanism for this, involving the transfer of feedback information to the ITC, ultimately resolving the issue of occluded face images in the second phase of the ITC.

The Coordination between the Frontal and Temporal Regions Is Associated with the Level of Occlusion. Consistent with prior research on the involvement of the vlPFC region in addressing challenging image-related issues (16, 17), we observed a higher PLV between the two areas (ITC and vlPFC) in the alpha-beta frequency range (7 to 17 Hz) when faces are more occluded compared to faces with a low level of occlusion. The alpha-beta frequency is recognized as a feedback index (25, 64–67).

The precise behavioral differentiation of occluded stimuli, along with a notable change in the response rate of the ITC, implies the involvement of the extra visual cortex such as the PFC in the representation of challenging objects. The observed frontotemporal coordination suggests the important role of the vlPFC in occlusion processing. While the vlPFC is not typically associated with passive tasks, recent studies highlight its role in the second phase of processing in non-task-dependent situations (23, 68, 69). However, the passive paradigm in our study makes our results less susceptible to the influence of various high-level confounds, such as attention, vigilance level, working memory, and other active components.

The reported neural mechanism is among the first studies that suggest the neural mechanism of occluded face processing. The suggested mechanism necessitates the revision on the current artificial object understanding models that usually missed the role of feedback and temporal dynamics of representation. Although previous causal studies were consistent with our results, the casual study with inactivation of the vlPFC will provide strong evidence that support the role of PFC feedback in challenging complex object representation.

The reported neural data are among the first studies that suggest the neural mechanism of occluded face processing. The suggested mechanism necessitates the revision on the current artificial object understanding models that usually missed the role of feedback and temporal dynamics of representation. Although previous causal studies were consistent with our results (16, 70, 71), the casual study with inactivation of the vlPFC will provide strong evidence that supports the role of PFC feedback in challenging complex object representation.

The Brain Compensates for Occlusion by Increasing Microsaccade Activity. In our passive task, we investigated microsaccades and pupil size as indicators of behavior. Our results align with previous studies showing that microsaccades help process difficult visual details (28, 72), especially when images are occluded (73, 74). We found that, from 200 ms into the second phase of ITC neuron responses, microsaccade activity increased significantly for occluded images compared to intact images. This finding supports our earlier results on how the brain processes occluded images. Additionally, it suggests that information about occlusion transmitted from the vlPFC to the ITC may influence microsaccade rates during this phase. This indicates that the brain uses enhanced microsaccade activity to gather additional visual information and sustain a continuous perception of the object.

Pupil size is a valuable indicator of brain state, providing insights into arousal and cognitive processes. Changes in pupil size reflect variations in neuromodulatory activity, which in turn affects how different brain structures process information. When pupil size increases or decreases, it signals shifts in the brain's arousal levels and cognitive states (75, 76). Pupil size is also influenced by stimulus properties like size, contrast, and spatial frequency. Larger stimuli typically cause more constriction, regardless of luminance (29, 30). Our results show that brain state, as measured by pupil size, remains unchanged when viewing different stimuli, such as intact and occluded face images. This consistency suggests that not only are the image characteristics similar, but the brain is also in a similar state regarding cognitive processing and arousal. The observed differences

in neural responses to intact vs. occluded faces are therefore likely due to differences in how these images are represented in the brain, rather than differences in cognitive load or arousal.

The finding that the PLV for occluded images was consistently higher than for intact images, regardless of pupil size, suggests that the observed neural differences are due to the way the brain processes occluded images, rather than being influenced by changes in brain state or arousal levels.

The reported neural mechanism is among the first studies that suggest the neural mechanism of occluded face processing. This finding necessitates a revision of current artificial object understanding models, which often overlook the role of feedback and the temporal dynamics of representation. Although previous causal studies were consistent with our results (16, 70, 71), a causal study involving vlPFC inactivation would provide strong evidence supporting the role of PFC feedback in challenging complex object representation.

One of the primary limitations of our study is the use of a passive viewing task, which does not directly assess how monkeys perceive or discriminate between intact and occluded faces. While the passive task allowed us to focus on the intrinsic neural coding within the ITC and vlPFC, it does not provide insights into how these neural responses translate into perceptual or behavioral outcomes. This limitation underscores the need for future studies to incorporate behavioral measures or active tasks to further explore the relationship between perception and neural activity in these regions. Additionally, a limitation of this study is the lack of fMRI to define face-selective patches, making it challenging to precisely identify the specific neuronal populations within the ITC from which we recorded. This limitation underscores the importance of future studies combining stereotaxic methods with fMRI to achieve more accurate localization of face-selective neurons.

Materials and Methods

Animal. Two adult male rhesus macaques (Macaca mulatta), Monkey J (7 y old, 10 kg) and Monkey Z (14 y old, 12 kg), were used in the study. MRI and CT scans were used to position recording chambers over the ITC and vlPFC. Chambers were implanted surgically under isoflurane anesthesia. The experimental protocols were approved by the Institute's Fundamental Science committee (99/60/1/160/1).

Neurophysiology. Extracellular recordings of spike activity and local field potentials (LFPs) were conducted using single electrodes in the vlPFC and ITC regions. Data were collected from 161 vlPFC neurons (109 from Monkey J and 52 from Monkey Z) and 184 IT neurons (132 from Monkey J and 52 from Monkey Z). Neural regions were identified based on stereotaxic coordinates, sulci patterns, and responses to electrical stimulation.

Stimuli. We used two sets of grayscale stimuli for the study: The first set comprised 165 photographs for selectivity tests (e.g., faces, bodies, natural and man-made objects), while the second set included 392 photographs with human and monkey faces, along with natural and artificial occluders. Natural occluders (e.g., masks, glasses, caps) and artificial ones (e.g., phase, texture, pixel scramble) were employed to investigate the effects of occlusion on neural responses. Stimuli were matched for luminance and contrast using the Shine Toolbox (50), and presented in a randomized sequence.

Behavioral. Monkeys were trained to perform a passive fixation task while seated in primate chairs with their heads restrained. Visual stimuli were displayed for 350 ms on an LED monitor, and juice rewards were provided every 3 to 5 s during successful fixation. Eye position was monitored using an infrared eye tracker (EyeLink 1000 Plus, SR Research Ltd.). The face-selectivity index was used to identify face-selective neurons in the ITC, and only face-selective neurons were prioritized for recording in the vlPFC.

Data Analysis. Data analysis was conducted using MATLAB (MathWorks) with the exception of Granger causality analysis, which was performed in Python. Raw LFP data were filtered between 1 and 300 Hz and resampled at 1 kHz. LFP data were normalized by subtracting the mean and dividing by the SD across trials. For firing rate analysis, spike trains were smoothed using a 10 ms Gaussian kernel. Normalized firing rates and face-selectivity indices were calculated to assess neuronal responses. Peak response times were determined using the MATLAB "findpeaks" function within 50 to 600 ms poststimulus onset.

Tuning Curve. To analyze neuronal tuning, we normalized all responses and computed the mean response at each occlusion level. For each neuron, we fitted a GLM across four occlusion levels. The slope of the fitted line indicated the neuron's preference for either occluded or intact faces, with positive slopes reflecting a preference for occluded faces and negative slopes for intact faces.

Representational Similarity Analysis (RSA). We applied RSA using a 50 ms sliding window with a 10 ms stride on spike trains to capture neural activity patterns. Correlation distance (1 minus linear correlation) was used to compute pairwise dissimilarity values (59, 60), resulting in a representational dissimilarity matrix (RDM). Four computational models, each representing different levels of occlusion, were compared with brain RDMs using Spearman rank correlation to assess the similarity between the observed neural representations and the theoretical models.

Regression Model. We employed a GLM to assess the relationship between neural responses and the level of occlusion. To ensure accurate results, we regressed out the effects of overall luminance, contrast, and identity information. Contrast was calculated for each stimulus, and principal components of image features were included in the GLM to model primitive stimulus characteristics.

Classification Accuracy (SVM) Over Time. To assess how classification accuracy evolves over time, we used a 50 ms sliding window with 5 ms steps. An SVM classifier with a linear kernel was trained on 70% of the data and tested on 30%, with normalization of accuracy reported to account for chance levels (77). SE were calculated based on 500 repetitions of random partitioning into training and test sets.

Time–Time Decoding. Neural activity data were used to train SVM classifiers to differentiate between occlusion levels at each time point. The classifiers were tested for their ability to generalize across all time points, evaluating their predictive performance beyond the training windows (78).

Granger Causality. We used Granger causality analysis to investigate the functional coordination between ITC and vlPFC circuits. This method involves training autoregressive models on RDMs from each brain area to forecast subsequent time steps (79). The ratio of unexplained variance between models trained on single vs. combined areas quantifies directional influence, allowing us to assess the functional interaction between regions.

PLV. Synchronization between signals was assessed using the PLV. Data were filtered in the alpha-beta band (7 to 17 Hz), and PLV was calculated based on the instantaneous phase of the signals. This measure quantifies the degree of synchronization between two signals, with values ranging from 0 (random phase relationship) to 1 (fixed phase relationship).

Statistical Analysis. Statistical analyses were performed using the Wilcoxon signed-rank test for paired comparisons and the rank-sum test for unpaired comparisons, unless otherwise specified. Comparisons were conducted across the population. For example, in comparing PLV between fully occluded and intact trials, the Wilcoxon signed-rank test was employed. Results include SEM, and permutation *P*-values were calculated with a specified number of iterations.

Data, Materials, and Software Availability. The data, analysis, and related materials are available in Github (80). All other data are included in the article and/or *SI Appendix*.

ACKNOWLEDGMENTS. The authors gratefully acknowledge the support provided by the Iran National Science Foundation (INSF), which funded this work under project No. 4022521. This support has been instrumental in advancing our research objectives and enabling the successful completion of this study. We extend our appreciation to INSF for its commitment to fostering scientific innovation and excellence.

Author affiliations: [a]Department of Physiology, Faculty of Medical Sciences, Tarbiat Modares University, Tehran 14115-111, Iran; [b]School of Cognitive Sciences, Institute for Research in Fundamental Sciences, Tehran 19395-5746, Iran; [c]Department of Psychology, Faculty of Psychology and Education, University of Tehran, Tehran 14155-6456, Iran; and [d]School of Electrical and Computer Engineering, College of Engineering, University of Tehran, Tehran 14395-515, Iran

1. A. M. Burton, R. Jenkins, P. J. Hancock, D. White, Robust representations for face recognition: The power of averages. *Cogn. Psychol.* **51**, 256–284 (2005).
2. C. Jacques *et al.*, The neural basis of rapid unfamiliar face individuation with human intracerebral recordings. *Neuroimage* **221**, 117174 (2020).
3. J. Taubert, K. B. Weldon, L. A. Parr, Robust representations of individual faces in chimpanzees (Pan troglodytes) but not monkeys (Macaca mulatta). *Anim. Cogn.* **20**, 321–329 (2017).
4. A. Thatere, A. Meshram, P. Verma, A. Jirapure, Eds., "Face recognition under occlusion: An efficient handcrafted feature & SVM based approach" in *2024 IEEE International Conference on Interdisciplinary Approaches in Technology and Management for Social Innovation (IATMSI)*, A. Thatere, A. Meshram, P. Verma, A. Jirapure, Eds. (IEEE, 2024).
5. M. Fu, Z. Wang, D. Fan, H. Wu, Eds., "Occlusion face recognition based on improved attention mechanism" in *International Conference on Computer Graphics, Artificial Intelligence, and Data Processing (ICCAID 2022)*, M. Fu, Z. Wang, D. Fan, H. Wu, Eds. (SPIE, 2023).
6. S.-R. Afraz, R. Kiani, H. Esteky, Microstimulation of inferotemporal cortex influences face categorization. *Nature* **442**, 692–695 (2006).
7. S. Sadagopan, W. Zarco, W. A. Freiwald, A causal relationship between face-patch activity and face-detection behavior. *Elife* **6**, e18558 (2017).
8. R. Azadi, E. Lopez, J. Taubert, A. Patterson, A. Afraz, Inactivation of face-selective neurons alters eye movements when free viewing faces. *Proc. Natl. Acad. Sci. U.S.A.* **121**, e2309906121 (2024).
9. G. Schalk *et al.*, Facephenes and rainbows: Causal evidence for functional and anatomical specificity of face and color processing in the human brain. *Proc. Natl. Acad. Sci. U.S.A.* **114**, 12285–12290 (2017).
10. T. Namima, A. Pasupathy, Encoding of partially occluded and occluding objects in primate inferior temporal cortex. *J. Neurosci.* **41**, 5652–5666 (2021).
11. G. Kovács, R. Vogels, G. A. Orban, Selectivity of macaque inferior temporal neurons for partially occluded shapes. *J. Neurosci.* **15**, 1984–1997 (1995).
12. Y. Kosai, Y. El-Shamayleh, A. M. Fyall, A. Pasupathy, The role of visual area V4 in the discrimination of partially occluded shapes. *J. Neurosci.* **34**, 8570–8584 (2014).
13. E. B. Issa, J. J. DiCarlo, Precedence of the eye region in neural processing of faces. *J. Neurosci.* **32**, 16666–16682 (2012).
14. D. Y. Tsao, N. Schweers, S. Moeller, W. A. Freiwald, Patches of face-selective cortex in the macaque frontal lobe. *Nat. Neurosci.* **11**, 877 (2008).
15. E. K. Miller, J. D. Cohen, An integrative theory of prefrontal cortex function. *Annu. Rev. Neurosci.* **24**, 167–202 (2001).
16. K. Kar, J. J. DiCarlo, Fast recurrent processing via ventrolateral prefrontal cortex is needed by the primate ventral stream for robust core visual object recognition. *Neuron* **109**, 164–176.e5 (2021).
17. A. M. Fyall, Y. El-Shamayleh, H. Choi, E. Shea-Brown, A. Pasupathy, Dynamic representation of partially occluded objects in primate prefrontal and visual cortex. *Elife* **6**, e25784 (2017).
18. J. Liu, M. Higuchi, A. Marantz, N. Kanwisher, The selectivity of the occipitotemporal M170 for faces. *Neuroreport* **11**, 337–341 (2000).
19. J. Liu, A. Harris, N. Kanwisher, Stages of processing in face perception: An MEG study. *Nat. Neurosci.* **5**, 910–916 (2002).
20. S. M. Crouzet, H. Kirchner, S. J. Thorpe, Fast saccades toward faces: Face detection in just 100 ms. *J. Vis.* **10**, 16.1–16.7 (2010).
21. S. M. Crouzet, S. J. Thorpe, Low-level cues and ultra-fast face detection. *Front. Psychol.* **2**, 342 (2011).
22. W. A. Freiwald, D. Y. Tsao, M. S. Livingstone, A face feature space in the macaque temporal lobe. *Nat. Neurosci.* **12**, 1187 (2009).
23. K. Kar, J. Kubilius, K. Schmidt, E. B. Issa, J. J. DiCarlo, Evidence that recurrent circuits are critical to the ventral stream's execution of core object recognition behavior. *Nat. Neurosci.* **22**, 974–983 (2019).
24. N. Kriegeskorte, M. Mur, P. Bandettini, Representational similarity analysis–Connecting the branches of systems neuroscience. *Front. Syst. Neurosci.* **2**, 4 (2008).
25. Z. Bahmani, M. R. Daliri, Y. Merrikhi, K. Clark, B. Noudoost, Working memory enhances cortical representations via spatially specific coordination of spike times. *Neuron* **97**, 967–979.e6 (2018).
26. N. Zammit, O. Falzon, K. Camilleri, R. Muscat, Working memory alpha–beta band oscillatory signatures in adolescents and young adults. *Eur. J. Neurosci.* **48**, 2527–2536 (2018).
27. C. Tallon-Baudry, S. Mandon, W. A. Freiwald, A. K. Kreiter, Oscillatory synchrony in the monkey temporal lobe correlates with performance in a visual short-term memory task. *Cereb. Cortex* **14**, 713–720 (2004).
28. R. Engbert, R. Kliegl, Microsaccades uncover the orientation of covert attention. *Vision Res.* **43**, 1035–1045 (2003).
29. J. Gao, A. Ko, Y. Yabe, M. A. Goodale, J. Chen, Pupil size is modulated by the size of equal-luminance gratings. *J. Vis.* **20**, 4 (2020).
30. J. H. Kim, C. Yin, E. P. Merriam, Z. N. Roth, Pupil size is sensitive to low-level stimulus features, independent of arousal-related modulation. *eNeuro* **10**, ENEURO.0005-23.2023 (2023).
31. F. Kraus, S. Tune, J. Obleser, B. Herrmann, Neural α oscillations and pupil size differentially index cognitive demand under competing audiovisual task conditions. *J. Neurosci.* **43**, 4352–4364 (2023).
32. K. V. Jakobsen, C. White, E. A. Simpson, General and own-species attentional face biases. *Atten. Percept. Psychophys.* **83**, 187–198 (2021).
33. Y. Qian, K. S. Scherf, Mapping the neural mechanisms of the own species bias in the ventrovisual pathway. *J. Vis.* **22**, 4406 (2022).
34. N. Bruno, M. Bertamini, F. Domini, Amodal completion of partly occluded surfaces: Is there a mosaic stage? *J. Exp. Psychol. Hum. Percept. Perform.* **23**, 1412–1426 (1997).
35. A. B. Sekuler, S. E. Palmer, Perception of partly occluded objects: A microgenetic analysis. *J. Exp. Psychol. Gen.* **121**, 95–111 (1992).
36. P. J. Kellman, E. S. Spelke, Perception of partly occluded objects in infancy. *Cogn. Psychol.* **15**, 483–524 (1983).
37. K. C. Soska, K. E. Adolph, S. P. Johnson, Systems in development: Motor skill acquisition facilitates three-dimensional object completion. *Dev. Psychol.* **46**, 129–138 (2010).
38. S. Vrins, S. Hunnius, R. van Lier, Volume completion in 4.5-month-old infants. *Acta Psychol. (Amst)* **138**, 92–99 (2011).
39. P. van Geert, A dynamic systems model of basic developmental mechanisms: Piaget, Vygotsky, and beyond. *Psychol. Rev.* **105**, 634–677 (1998).
40. J. Thielen, S. E. Bosch, T. M. van Leeuwen, M. A. J. van Gerven, R. van Lier, Neuroimaging findings on amodal completion: A review. *Iperception* **10**, 2041669519840047 (2019).
41. J. A. Assad, J. H. Maunsell, Neuronal correlates of inferred motion in primate posterior parietal cortex. *Nature* **373**, 518–521 (1995).
42. O. J. Hulme, S. Zeki, The sightless view: Neural correlates of occluded objects. *Cereb. Cortex* **17**, 1197–1205 (2007).
43. G. Erlikhman, G. P. Caplovitz, Decoding information about dynamically occluded objects in visual cortex. *Neuroimage* **146**, 778–788 (2017).
44. C. I. Baker *et al.*, Neuronal representation of disappearing and hidden objects in temporal cortex of the macaque. *Exp. Brain Res.* **140**, 375–381 (2001).
45. J. Chen, T. Zhou, H. Yang, F. Fang, Cortical dynamics underlying face completion in human visual system. *J. Neurosci.* **30**, 16692–16698 (2010).
46. N. Kanwisher, G. Yovel, The fusiform face area: A cortical region specialized for the perception of faces. *Philos. Trans. R. Soc. Lond. B Biol. Sci.* **361**, 2109–2128 (2006).
47. C. Yin, S. Shimojo, C. Moore, S. A. Engel, Dynamic shape integration in extrastriate cortex. *Curr. Biol.* **12**, 1379–1385 (2002).
48. M. A. Umiltà *et al.*, I know what you are doing. a neurophysiological study. *Neuron* **31**, 155–165 (2001).
49. D. Y. Tsao, W. A. Freiwald, T. A. Knutsen, J. B. Mandeville, R. B. Tootell, Faces and objects in macaque cerebral cortex. *Nat. Neurosci.* **6**, 989–995 (2003).
50. D. A. Leopold, I. V. Bondar, M. A. Giese, Norm-based face encoding by single neurons in the monkey inferotemporal cortex. *Nature* **442**, 572–575 (2006).
51. D. Tsao, A dedicated system for processing faces. *Science* **314**, 72–73 (2006).
52. S. Moeller, W. A. Freiwald, D. Y. Tsao, Patches with links: A unified system for processing faces in the macaque temporal lobe. *Science* **320**, 1355–1359 (2008).
53. M.-R. A. Dehaqani *et al.*, Temporal dynamics of visual category representation in the macaque inferior temporal cortex. *J. Neurophysiol.* **116**, 587–601 (2016).
54. E. Vul, D. Lashkari, P. J. Hsieh, P. Golland, N. Kanwisher, Data-driven functional clustering reveals dominance of face, place, and body selectivity in the ventral visual pathway. *J. Neurophysiol.* **108**, 2306–2322 (2012).
55. G. Kreiman *et al.*, Object selectivity of local field potentials and spikes in the macaque inferior temporal cortex. *Neuron* **49**, 433–445 (2006).
56. H. Komatsu, Y. Ideura, S. Kaji, S. Yamane, Color selectivity of neurons in the inferior temporal cortex of the awake macaque monkey. *J. Neurosci.* **12**, 408–424 (1992).
57. T. S. Lee, M. Nguyen, Dynamics of subjective contour formation in the early visual cortex. *Proc. Natl. Acad. Sci. U.S.A.* **98**, 1907–1911 (2001).
58. K. J. Nielsen, N. K. Logothetis, G. Rainer, Dissociation between local field potentials and spiking activity in macaque inferior temporal cortex reveals diagnosticity-based encoding of complex objects. *J. Neurosci.* **26**, 9639–9645 (2006).
59. M. Bar, A cortical mechanism for triggering top-down facilitation in visual object recognition. *J. Cogn. Neurosci.* **15**, 600–609 (2003).
60. D. J. Kravitz, K. S. Saleem, C. I. Baker, L. G. Ungerleider, M. Mishkin, The ventral visual pathway: An expanded neural framework for the processing of object quality. *Trends Cogn. Sci.* **17**, 26–49 (2013).
61. H. Tomita, M. Ohbayashi, K. Nakahara, I. Hasegawa, Y. Miyashita, Top-down signal from prefrontal cortex in executive control of memory retrieval. *Nature* **401**, 699–703 (1999).
62. L. G. Ungerleider, T. W. Galkin, R. Desimone, R. Gattass, Cortical connections of area V4 in the macaque. *Cereb. Cortex* **18**, 477–499 (2007).
63. H. Barbas, M. M. Mesulam, Cortical afferent input to the principalis region of the rhesus monkey. *Neuroscience* **15**, 619–637 (1985).
64. T. van Kerkoerle *et al.*, Alpha and gamma oscillations characterize feedback and feedforward processing in monkey visual cortex. *Proc. Natl. Acad. Sci. U.S.A.* **111**, 14332–14341 (2014).
65. G. Michalareas *et al.*, Alpha-beta and gamma rhythms subserve feedback and feedforward influences among human visual cortical areas. *Neuron* **89**, 384–397 (2016).
66. C. G. Richter, W. H. Thompson, C. A. Bosman, P. Fries, Top-down beta enhances bottom-up gamma. *J. Neurosci.* **37**, 6698–6711 (2017).
67. T. Popov, S. Kastner, O. Jensen, FEF-controlled alpha delay activity precedes stimulus-induced gamma-band activity in visual cortex. *J. Neurosci.* **37**, 4117–4127 (2017).
68. J. L. McKee, M. Riesenhuber, E. K. Miller, D. J. Freedman, Task dependence of visual and category representations in prefrontal and inferior temporal cortices. *J. Neurosci.* **34**, 16065–16075 (2014).
69. L. Bugatus, K. S. Weiner, K. Grill-Spector, Task alters category representations in prefrontal but not high-level visual cortex. *Neuroimage* **155**, 437–449 (2017).
70. J. M. Hupé *et al.*, Cortical feedback improves discrimination between figure and background by V1, V2 and V3 neurons. *Nature* **394**, 784–787 (1998).
71. J. M. Fuster, R. H. Bauer, J. P. Jervey, Functional interactions between inferotemporal and prefrontal cortex in a cognitive task. *Brain Res.* **330**, 299–307 (1985).
72. S. Martinez-Conde, S. L. Macknik, X. G. Troncoso, T. A. Dyar, Microsaccades counteract visual fading during fixation. *Neuron* **49**, 297–305 (2006).
73. H. Palmieri, A. Fernández, M. Carrasco, Microsaccades and temporal attention at different locations of the visual field. *J. Vis.* **23**, 6 (2023).
74. T. Tammi, J. Pekkanen, S. Tuhkanen, L. Oksama, O. Lappi, Tracking an occluded visual target with sequences of saccades. *J. Vis.* **22**, 9 (2022).
75. L. Hong, J. M. Walz, P. Sajda, Your eyes give you away: Prestimulus changes in pupil diameter correlate with poststimulus task-related EEG dynamics. *PLoS One* **9**, e91321 (2014).
76. R. Montefusco-Siegmund *et al.*, Alpha EEG activity and pupil diameter coupling during inactive wakefulness in humans. *eNeuro* **9**, ENEURO.0060-21.2022 (2022).
77. V. N. Vapnik, Ed., "The Support Vector method" in *Artificial Neural Networks–ICANN'97*, V. N. Vapnik, Ed. (Springer Berlin Heidelberg, Berlin, Heidelberg, 1997).
78. R. M. Cichy, D. Pantazis, A. Oliva, Resolving human object recognition in space and time. *Nat. Neurosci.* **17**, 455–462 (2014).
79. T. C. Kietzmann *et al.*, Recurrence is required to capture the representational dynamics of the human visual system. *Proc. Natl. Acad. Sci. U.S.A.* **116**, 21854–21863 (2019).
80. J. Noroozi, jalaledin/Occlusion-Faces. GitHub. https://github.com/jalaledin/Occlusion-Faces. Accessed 5 November 2024.